

The Method of Comparison Equations for Schwarzschild Black Holes

Roberto Casadio^{1,*} and Mattia Luzzi^{1,†}

¹*Dipartimento di Fisica, Università di Bologna and I.N.F.N.,
Sezione di Bologna, via Irnerio 46, 40126 Bologna, Italy.*

We employ the method of comparison equations to study the propagation of a massless minimally coupled scalar field on the Schwarzschild background. In particular, we show that this method allows us to obtain explicit approximate expressions for the radial modes with energy below the peak of the effective potential which are fairly accurate over the whole region outside the horizon. This case can be of particular interesting, for example, for the problem of black hole evaporation.

PACS numbers: 98.80.Cq, 98.80.-k

I. INTRODUCTION

Wave equations on black hole backgrounds cannot be solved exactly in terms of known simple functions (for a review, see, *e.g.*, Ref. [1]). Although it is usually fairly easy to find asymptotic expressions near the (outer) horizon or at spatial infinity, numerical analysis is what one eventually employs to obtain a detailed profile of the wave-functions. However, our understanding of the field dynamics on curved backgrounds would still benefit of analytical approximations to the exact modes, for example in the study of the (renormalized) energy-momentum tensor of quantum fields [2] and, in particular, of the Hawking radiation [3], or of quasi-normal modes [4].

By making use of the black hole symmetry, one can usually separate the wave-functions and reduce the problem to the one task of solving a second order differential equation for the radial part. The latter takes the form of the one-dimensional Schrödinger equation for the transmission through a potential barrier [1]

$$\left[\frac{d^2}{dx^2} + Q_s(x) \right] \psi = 0, \quad (1)$$

and, for the general case of a Kerr-Newman black hole, is known as the Teukolsky master equation for waves of spin-weight $s = 0, 1$ and 2 [1, 5].

A well known method to solve equations of the form (1) is the Wentzel-Kramers-Brillouin (WKB) approximation [6, 7], which has in fact been widely used to study wave equations on black hole backgrounds (for one of the first attempts see Ref. [8] and for recent reviews see, *e.g.*, Ref. [9] and References therein). One of the weaknesses of this method is that it becomes rather cumbersome near the “turning points”, that is where the potential vanishes and one must match different branches of approximate solutions. The precise location of the matching points greatly affects the accuracy of the method and may lead to errors at next-to-leading order larger than those at leading order (for a detailed analysis of this point in the

context of cosmology, see Ref. [10]). The fact that the potentials in the radial equations on black hole backgrounds can in general have two turning points makes therefore it difficult to apply the WKB approximation.

There are however improved versions of the WKB approximation and, in the present paper, we shall concentrate on the one which seems to give the most accurate leading order expressions. The method of comparison equations (MCE) was independently introduced in Refs. [11, 12] and later applied, for example, to wave mechanics [13] and cosmology [14]. Its connection with the Ermakov-Pinney equation was also studied in Ref. [15]. Its strength consists in yielding approximate modes which are rather accurate over the entire domain of definition of the wave-functions. The approximate wave-functions are however given in terms of a new independent variable and computing their explicit dependence on the original variable is now the most difficult task which requires a good deal of trial-and-error work.

In the next Section, we shall briefly review the equation of motion for massless scalar fields on a spherically symmetric black hole background. This includes the simplest case of linear scalar perturbations of a Schwarzschild black hole which will be used to show the application of our method in all details (including the use of a convenient radial coordinate and rescaling of the wave-function). In Section III, we shall then apply the MCE and obtain approximate expressions for scalar wave-modes with energy below the peak of the potential. This case is of particular interest, for example, for evaluating the grey-body factors involved in the Hawking effect [3]. It also presents a major complication with respect to the typical cases treated in Ref. [14], namely the presence of two zeros of the potential (“turning points”). We shall use units with $c = G = 1$.

II. SCALAR FIELD ON SCHWARZSCHILD BACKGROUND

Let us begin by recalling that the metric in a static and spherically symmetric vacuum space-time can be written

*Electronic address: Roberto.Casadio@bo.infn.it

†Electronic address: Mattia.Luzzi@bo.infn.it

in general as

$$ds^2 = h(r) dt^2 - \frac{dr^2}{h(r)} - r^2 d\Omega^2, \quad (2)$$

where $d\Omega$ is the area element on the unit two-sphere. The propagation of massless, minimally coupled scalar particles in this background is governed by the Klein-Gordon equation $\Phi^{;\mu}_{;\mu} = 0$. Due to the symmetry of the background, the field Φ can be decomposed into eigenmodes of normal frequency $\tilde{\omega}$ and angular momentum numbers ℓ, m as [1]

$$\Phi(t, r, \Omega) = e^{-i\tilde{\omega}t} Y_\ell^m(\Omega) R(r), \quad (3)$$

where Y_ℓ^m are spherical harmonics. The Klein-Gordon equation then separates and the dynamics is described by the function R which satisfies the radial equation

$$\frac{d}{dr} \left[r^2 h(r) \frac{dR(r)}{dr} \right] + \left[\frac{\tilde{\omega}^2 r^2}{h(r)} - \ell(\ell+1) \right] R(r) = 0, \quad (4)$$

where $\ell(\ell+1)$ is the separation constant. No exact solution of the above equation is known even for as simple a

background as the four-dimensional Schwarzschild space-time with

$$h(r) = 1 - \tilde{r}^{-1}, \quad (5)$$

where we have introduced the dimensionless radial coordinate $\tilde{r} = r/r_H$ and r_H is the Schwarzschild radius.

It is now convenient to introduce the ‘‘tortoise-like’’ coordinate [24]

$$dx = \frac{d\tilde{r}}{\tilde{r} h(\tilde{r})}, \quad (6a)$$

and the new radial function

$$R[\tilde{r}(x)] = \exp \left[-\frac{1}{2} \int^x h(x') dx' \right] \chi[\tilde{r}(x)], \quad (6b)$$

so that the radial equation takes the Schrödinger form

$$\frac{d^2 \chi(x)}{dx^2} + \left\{ \tilde{\omega}^2 \tilde{r}^2(x) - \ell(\ell+1) h[\tilde{r}(x)] - \frac{1}{4} h^2[\tilde{r}(x)] - \frac{1}{2} \frac{dh[\tilde{r}(x)]}{dx} \right\} \chi(x) = 0. \quad (7)$$

where we also defined the dimensionless energy $\tilde{\omega} \equiv \tilde{\omega} r_H$. For the four-dimensional Schwarzschild case we have

$$x(\tilde{r}) = \ln(\tilde{r} - 1), \quad (8)$$

so that the new variable x ranges from $x(\tilde{r}_H = 1) = -\infty$ to $x(\tilde{r} = +\infty) = +\infty$ and x and $\chi(x)$ are of Langer’s form [7]. The Klein-Gordon equation finally becomes

$$\left[\frac{d^2}{dx^2} + \omega^2(x) \right] \chi(x) = 0, \quad (9)$$

where the ‘‘frequency’’

$$\omega^2(x) = \tilde{\omega}^2 (1 + e^x)^2 - \frac{\ell(\ell+1) e^x}{1 + e^x} - \frac{e^x (2 + e^x)}{4 (1 + e^x)^2}, \quad (10)$$

is not necessarily a positive quantity. In fact, the above expression shows two qualitatively different behaviors depending on the values of $\tilde{\omega}$ and ℓ . In particular, for a given angular momentum ℓ , there exists a critical value

$$\tilde{\omega}_c = \tilde{\omega}_c(\ell), \quad (11)$$

such that if the energy $\tilde{\omega} > \tilde{\omega}_c$ there are no turning points, otherwise there are two, say $\omega(x_1) = \omega(x_2) = 0$ with $x_1 < x_2$. The latter case is the one we want to analyze in detail (see Appendix A for more details and the solid line in Fig. 1 for an example).

III. MCE SOLUTIONS

The MCE makes use of the exact solutions to a similar second-order differential equation,

$$\left[\frac{d^2}{d\bar{\sigma}^2} + \Theta^2(\bar{\sigma}) \right] U(\bar{\sigma}) = 0, \quad (12)$$

where Θ is the ‘‘comparison function’’. One can then represent exact solutions of Eq. (9) in the form

$$\chi(x) = \left(\frac{d\bar{\sigma}}{dx} \right)^{-1/2} U(\bar{\sigma}), \quad (13)$$

provided the variables $\bar{\sigma}$ and x are related by

$$\omega^2(x) = \left(\frac{d\bar{\sigma}}{dx} \right)^2 \Theta^2(\bar{\sigma}) - \left(\frac{d\bar{\sigma}}{dx} \right)^{1/2} \frac{d^2}{dx^2} \left(\frac{d\bar{\sigma}}{dx} \right)^{-1/2}. \quad (14)$$

Of course, solving Eq. (14) is usually as difficult as the original problem (9), and the dependence of $\bar{\sigma}$ on x can just be determined by using iterative schemes, in general cases [15, 16] or for specific problems [17, 18]. However, if we are able to find a comparison function Θ sufficiently similar to ω in Eq. (10), the second term in the right hand side of Eq. (14) will be negligible with respect to

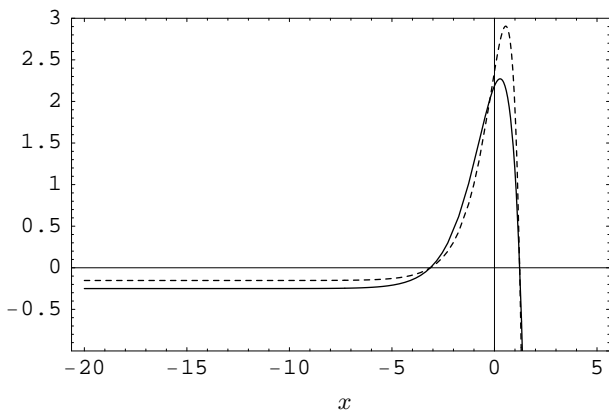


FIG. 1: Comparison between the exact potential $-\omega^2(x)$ (solid line) and the approximate Morse potential $-\Theta^2[\sigma(x)]$ obtained after solving Eqs. (19a) and (19b) (dotted line) for $\tilde{\omega} = 1/2$ and $\ell = 2$. The two turning points are $x_1 \approx -3.13$ and $x_2 \approx 1.23$.

the first one, so that

$$\omega^2(x) \simeq \left(\frac{d\bar{\sigma}}{dx} \right)^2 \Theta^2(\bar{\sigma}). \quad (15)$$

On selecting a pair of values x_0 and $\bar{\sigma}_0$ such that $\bar{\sigma}_0 = \bar{\sigma}(x_0)$, the function $\bar{\sigma}(x)$ can then be approximated by a solution $\sigma = \sigma(x)$ of the integral equation

$$\int_{x_0}^x \sqrt{\pm \omega^2(y)} dy = \int_{\sigma_0}^{\sigma} \sqrt{\pm \Theta^2(\rho)} d\rho, \quad (16)$$

where the signs must be chosen conveniently. This procedure leads to the MCE approximation for $\chi(x)$,

$$\chi_{\text{MCE}}(x) = \left(\frac{d\sigma}{dx} \right)^{-1/2} U(\sigma), \quad (17)$$

which is valid in the whole range of x and including the turning points.

We are now dealing with a problem of the form (9) with two turning points, $x_1 < x_2$. In order to implement the MCE, we need a “comparison frequency” with the same behavior. We shall use the Morse potential [19]

$$\Theta^2(\sigma) = A e^{2\sigma} - B e^{\sigma} + D. \quad (18)$$

The coefficients A and B are then fixed by imposing that the turning points of the comparison function are the same as those of the exact frequency, that is

$$\Theta(\sigma_1 = x_1) = \Theta(\sigma_2 = x_2) = 0, \quad (19a)$$

and the coefficient D will then follow from the relation

$$\xi \equiv \int_{x_1}^{x_2} \sqrt{-\omega^2(y)} dy = \int_{x_1}^{x_2} \sqrt{-\Theta^2(\rho)} d\rho. \quad (19b)$$

The system of non-linear equations (19a) and (19b) thus yields

$$A = \frac{4\xi^2}{\pi^2 (w_1 + w_2 - 2\sqrt{w_1 w_2})^2} \quad (20a)$$

$$B = (w_1 + w_2) A \quad (20b)$$

$$D = w_1 w_2 A, \quad (20c)$$

where the exact expression for ξ is given in Appendix B. A sample plot of both the exact frequency and the comparison function thus obtained is given in Fig. 1.

The “comparison solution” is a linear combination of confluent hypergeometric functions [20] of the type ${}_1F_1$ (for more details, see Ref. [19]),

$$U(\sigma) = C_+ e^{i(\sqrt{A}e^\sigma + \sqrt{D}\sigma)} {}_1F_1\left(\frac{1}{2} + i\sqrt{D} + i\frac{B}{2\sqrt{A}}, 1 + 2i\sqrt{D}, -2i\sqrt{A}e^\sigma\right) + C_- e^{i(\sqrt{A}e^\sigma - \sqrt{D}\sigma)} {}_1F_1\left(\frac{1}{2} - i\sqrt{D} + i\frac{B}{2\sqrt{A}}, 1 - 2i\sqrt{D}, -2i\sqrt{A}e^\sigma\right) \quad (21)$$

and $\sigma(x)$ is given implicitly by Eq. (16) with

$$\int_{x_1}^{\sigma} \sqrt{\Theta^2(\rho)} d\rho = \sqrt{\Theta^2(\sigma)} - \ln \left[\left(2A e^\sigma - B + 2\sqrt{A\Theta^2(\sigma)} \right)^{\frac{B}{2\sqrt{A}}} \left(2D e^{-\sigma} - B + 2e^{-\sigma} \sqrt{D\Theta^2(\sigma)} \right)^{\sqrt{D}} \right]. \quad (22)$$

The above expression is rather complex. Hence, we just consider the asymptotic relation between σ and x to the

left of the smaller turning point (that is, for $x \ll x_1$)

$$\sigma(x) \simeq \frac{\tilde{\omega}}{\sqrt{D}} x \quad (23a)$$

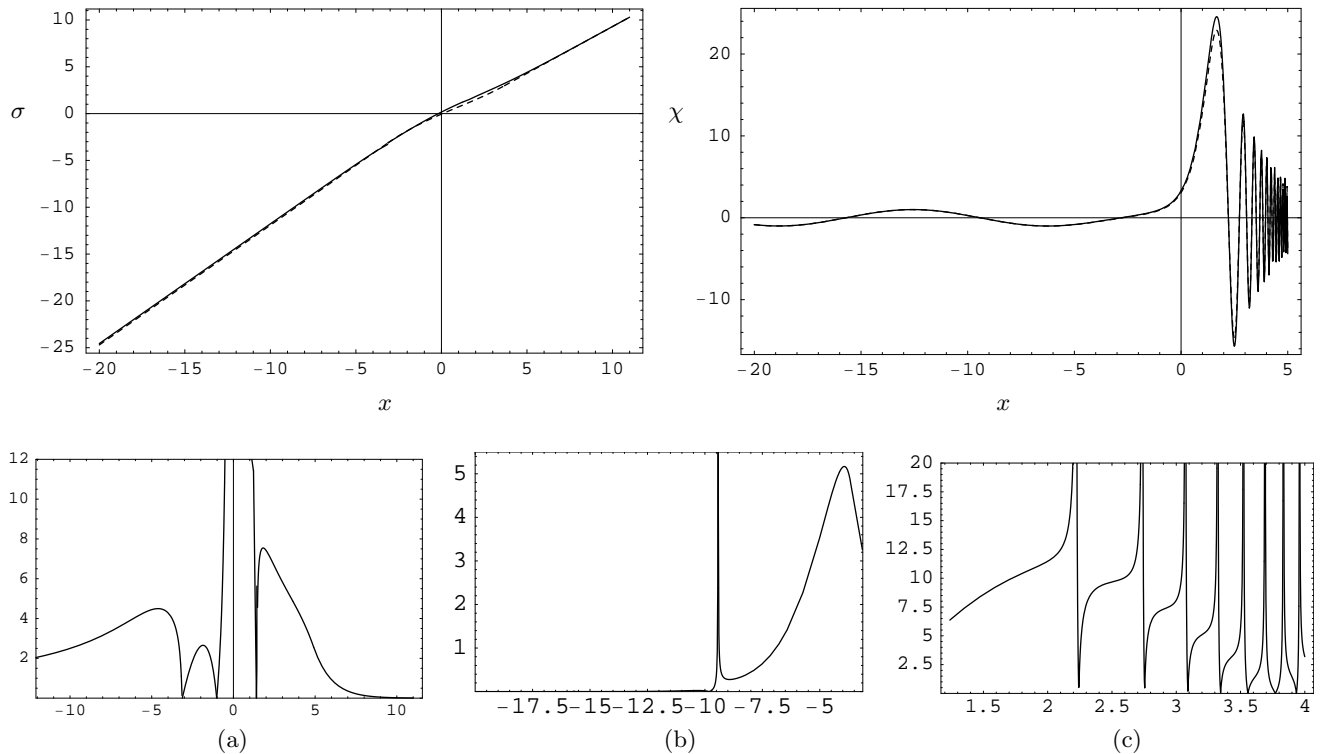


FIG. 2: Upper left graph: The function $\sigma = \sigma(x)$ obtained by integrating Eq. (16) numerically (solid line) and its approximate expression (24) with $\kappa_1 = 1$ and $\kappa_2 = 3$ (dashed line). Upper right graph: Comparison between the exact solution (solid line) and the approximate MCE solution (17) with $\sigma(x)$ evaluated numerically (dashed line) for $C_+ \approx 0.517 - 0.228i$ and $C_- \approx 0.517 + 0.228i$. Panel (a) shows the percentage error for the same approximate function σ given in the upper left graph. Panel (b) shows the percentage error for the approximate χ in the upper right graph for $x < x_1$ and panel (c) for $x_2 < x$. All plots are for $\tilde{\omega} = 1/2$, $\ell = 2$ as in Fig. 1.

and to the right of the larger one ($x \gg x_2$)

$$\sqrt{A}e^{\sigma(x)} - \frac{B}{2\sqrt{A}}\sigma(x) \simeq \tilde{\omega}(e^x + x). \quad (23b)$$

As an approximate expression for $\sigma(x)$ for $x < \kappa_1 x_1$ (with $\kappa_1 \gtrsim 1$) we shall then use Eq. (23a) and the condition that $\sigma(x_1) = x_1$. Analogously, for $x > \kappa_2 x_2$ (with $\kappa_2 \gtrsim 1$) we shall use the approximate solution of Eq. (23b) to next-to-leading order for large x . Moreover, in the region between $\kappa_1 x_1$ and $\kappa_2 x_2$ we shall use an interpolating cubic function. The reason for introducing two new parameters κ_1 and $\kappa_2 \gtrsim 1$ is that the asymptotic forms in Eqs. (23a) and (23b) may differ significantly from the correct $\sigma(x)$ around the turning points x_1 and x_2 and suitable values of κ_1 and κ_2 usually improve the final result. To summarize, we have

$$\sigma = \begin{cases} \frac{\tilde{\omega}}{\sqrt{D}}x + x_1 \left(1 - \frac{\tilde{\omega}}{\sqrt{D}}\right), & x_0 < x < \kappa_1 x_1 \\ C_0 + C_1 x + C_2 x^2 + C_3 x^3, & \kappa_1 x_1 < x < \kappa_2 x_2 \\ x + \ln \left(\frac{\tilde{\omega}}{\sqrt{A}}\right), & x > \kappa_2 x_2, \end{cases} \quad (24)$$

with κ_1 and $\kappa_2 \gtrsim 1$ and $x_0 < \kappa_1 x_1$ is the value of x at which we wish to impose the initial conditions for $\chi(x)$ and its derivative [25]. The explicit expressions for the coefficients C_0 , C_1 , C_2 and C_3 are rather cumbersome and will be given in Appendix C.

In the upper left panel of Fig. 2, we plot $\sigma(x)$ for the same values of $\tilde{\omega}$ and ℓ used in Fig. 1. The solid line represents the numerical solution of Eq. (16) and the dashed line the approximate expression (24) with $\kappa_1 = 1$ and $\kappa_2 = 3$. It is clear that these values of κ_1 and κ_2 already lead to a very good approximation for σ around the turning points x_1 and x_2 and that larger values of κ_1 or κ_2 would not improve significantly the final result. In the upper right panel of Fig. 2, we compare an MCE approximate wave-function with the exact solution (solid line) obtained numerically for the same case. The MCE solution shown by a dashed line is given by the expression (17) with $U(\sigma)$ as in Eq. (21) and $\sigma(x)$ determined by solving Eq. (16) numerically. The coefficients C_{\pm} are fixed by imposing that the MCE mode and its derivative equal the corresponding values of the chosen numerical solution at $x = -20$. Since the two curves coincide almost everywhere, it is clear that solving the approximate equation (16) for $\sigma(x)$ is, to all practical extents, equivalent to solving the original equation (9).

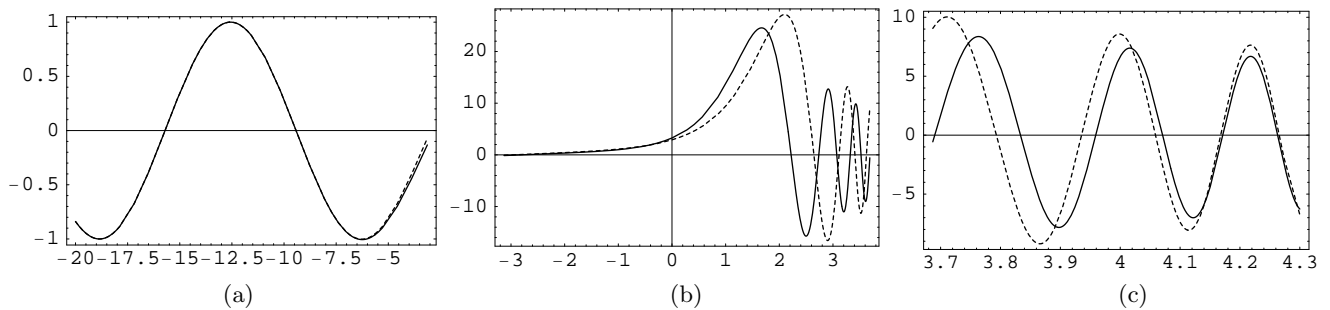


FIG. 3: Comparison between the exact solution (solid line) and the approximate MCE solution (17) with $\sigma(x)$ given in Eq. (24) with $\kappa_1 = 1$ and $\kappa_2 = 3$ (dashed line) for $\tilde{\omega} = 1/2$ and $\ell = 2$ (same as in Figs. 1 and 2). Panel (a) shows the result for $x < \kappa_1 x_1$, panel (b) for $\kappa_1 x_1 < x < \kappa_2 x_2$ and panel (c) for $x > \kappa_2 x_2$.

In order to further clarify this point, in panel (a) of Fig. 2, we plot the relative difference (in percent) between the approximate expression (24) and the exact numerical solution of Eq. (16). We can see that the error is less than 10% almost everywhere, except near the zero of $\sigma(x)$. In the same figure, we also show the percentage error for the approximate solution shown in the right upper graph of Fig. 2 for x on the left of x_1 and on the right of x_2 . The latter error remains small, too, except around the zeros of $\chi(x)$ due to the slight phase difference between the two expressions.

Finally, in Fig. 3, the dashed lines represent the same MCE solution with $\sigma(x)$ given by its analytical approximation in Eq. (24) with $\kappa_1 = 1$ and $\kappa_2 = 3$. This is the fully analytical expression obtained from the application of the MCE and is still remarkably good, with a more significant error around the larger turning point ($x_2 \approx 1.23$). From the three graphs in Fig. 3 and the upper left panel in Fig. 2, it clearly appears that such an error develops in the region between the two turning points, where the discrepancy between the exact $\sigma(x)$ and the approximate expression (24) is indeed larger. In this respect, let us note that, had we imposed initial conditions at $x \gg x_2$, the larger error would have occurred around the smaller turning point ($x_1 \approx -3.13$). Moreover, when we used a linear (or quadratic) interpolating function for $\kappa_1 x_1 < x < \kappa_2 x_2$, the accuracy was (expectedly) worse. Should one need even better accuracy, a fourth (or higher) order polynomial interpolation between $\kappa_1 x_1$ and $\kappa_2 x_2$ could be used instead.

IV. CONCLUSIONS

We have applied the method of comparison equations to a specific problem of scalar field dynamics on the Schwarzschild background. We have considered modes with energy lower than the peak of the effective potential in the corresponding wave equation, so that there are two zeros (turning points). The comparison function has then been chosen of the Morse form with an argument which we have estimated analytically as well. This procedure was shown to be able to produced a fully analytical

approximation of the wave-functions with good accuracy over the whole domain outside the Schwarzschild horizon.

Let us now make a few remarks. Firstly, the application of the MCE is not as straightforward as the standard WKB approximation. In fact, the MCE usually requires solving some technical tasks specific to the problem at hand in order to obtain the argument $\sigma = \sigma(x)$ of the known function $U = U(\sigma)$. This aspect has already been analyzed in the simpler situation of cosmological perturbations for which one needs consider just one turning point [14]. In the present case, with two turning points, all expressions become more involved. For instance, the best approximation for $\sigma(x)$ we found convenient to display in Eq. (24) makes use of a cubic interpolation over the region containing the two turning points and is given in terms of two arbitrary parameters κ_1 and κ_2 which can be fixed in order to minimize the error (and explicit expressions for the coefficients C_0, \dots, C_3 are given in Appendix C). Of course, one could employ higher order interpolating functions and further improve the result at the price of complexity if better accuracy is needed.

Finally, our aim for the present work was mainly to test the effectiveness of the MCE to produce approximate wave modes on black hole backgrounds. For this reason, no discussion of gauge fields, gravitational waves or spinors has been explicitly included. We in fact plan to apply the MCE also to such higher spin fields and further extend the method to study related problems, such as the quasi-normal modes [4] and grey-body factors [3] of radiating black holes (also in the brane-world [22], given the relevance of such objects in future collider experiments [23]).

APPENDIX A: TURNING POINTS

If we define $w = e^x$, we see that $\omega^2(x) = 0$ for the exact frequency in Eq. (10) becomes the quartic polynomial equation

$$w^4 + 4w^3 + bw^2 + cw + 1 = 0, \quad (\text{A1a})$$

with

$$b = 6 - \frac{1}{4\tilde{\omega}^2} - \frac{\ell(\ell+1)}{\tilde{\omega}^2} \quad (\text{A1b})$$

$$c = 4 - \frac{1}{2\tilde{\omega}^2} - \frac{\ell(\ell+1)}{\tilde{\omega}^2}. \quad (\text{A1c})$$

Its four roots can be written as

$$w_i = -1 + \frac{\epsilon_i}{2} \sqrt{4 - \frac{2}{3}b + \frac{\gamma}{3}} - \frac{\theta_i}{2} \sqrt{8 - \frac{4}{3}b + \epsilon_i \frac{4b - 16 - 2c}{\sqrt{4 - \frac{2}{3}b + \frac{\gamma}{3}}} - \frac{\gamma}{3}}, \quad (\text{A2a})$$

where $i = 1, \dots, 4$ and

$$\alpha = 12 + b^2 - 12c \quad (\text{A2b})$$

$$\beta = 2b^3 - 36bc + 27c^2 + 432 - 72b \quad (\text{A2c})$$

$$\gamma = \frac{2^{\frac{1}{3}} \alpha}{\left(\beta + \sqrt{\beta^2 - 4\alpha^3}\right)^{\frac{1}{3}}} + \frac{\left(\beta + \sqrt{\beta^2 - 4\alpha^3}\right)^{\frac{1}{3}}}{2^{\frac{1}{3}}}. \quad (\text{A2d})$$

The coefficients $\epsilon_1 = \epsilon_2 = -\epsilon_3 = -\epsilon_4 = \theta_1 = -\theta_2 = \theta_3 = -\theta_4 = 1$, and the values of $\tilde{\omega}$ and ℓ determine the signs of the roots. There can be at most two positive roots, in which case, say, $w_3 \leq w_4 \leq 0 \leq w_1 = e^{x_1} \leq w_2 = e^{x_2}$, and only x_1 and x_2 can be valid turning points. The critical value of $\tilde{\omega}$ in Eq. (11) is then determined by the condition $0 \leq w_1 = w_2$.

APPENDIX B: EVALUATION OF ξ

In order to evaluate the integral in Eq. (19b), we start from the general relation (again with $w = e^x$)

$$\begin{aligned} \frac{1}{\tilde{\omega}} \int_{x_1}^{\ln(w)} \sqrt{-\omega^2(y)} dy &= \sqrt{\frac{(w-w_3)(w-w_1)(w-w_2)}{w-w_4}} + \frac{1}{\sqrt{(w_1-w_3)(w_4-w_2)}} \\ &\times \left\{ (w_3-w_1)(w_4-w_2) E(z; W) - (w_4-w_1)(w_4-w_2) F(z; W) \right. \\ &\quad + (w_4-w_1)(w_3+w_4+w_1+w_2+2) \Pi\left[\frac{w_1-w_2}{w_4-w_2}; z; W\right] \\ &\quad - 2(w_4-w_1)(w_3+1)(w_2+1) \Pi\left[\frac{(w_4+1)(w_1-w_2)}{(w_1+1)(w_4-w_2)}; z; W\right] \\ &\quad \left. + 2(w_4-w_1)w_3w_2 \Pi\left[\frac{w_4(w_1-w_2)}{w_1(w_4-w_2)}; z; W\right] \right\}, \quad (\text{B1}) \end{aligned}$$

where E, F and Π are elliptic functions [20],

$$z = \text{ArcSin} \left[\sqrt{\frac{(w-w_1)(w_4-w_2)}{(w-w_4)(w_1-w_2)}} \right], \quad (\text{B2})$$

$$W = \frac{(w_3-w_4)(w_1-w_2)}{(w_3-w_1)(w_4-w_2)}, \quad (\text{B3})$$

and $w_i = e^{x_i}$ are the roots of $\omega^2(x)$ as given in the previous Appendix. The above expression evaluated at

$w = w_2$ yields

$$\begin{aligned} \xi &= \frac{\tilde{\omega}}{\sqrt{(w_1-w_3)(w_4-w_2)}} \\ &\times \left\{ (w_3-w_1)(w_4-w_3) E(W) \right. \\ &\quad + (w_4-w_1)(w_2-w_4) K(W) \\ &\quad + (w_4-w_1)(w_3+w_4+w_1+w_2+2) \Pi\left[\frac{w_1-w_2}{w_4-w_2}; W\right] \\ &\quad - 2(w_3+1)(w_2+1)(w_4-w_1) \Pi\left[\frac{(w_4+1)(w_1-w_2)}{(w_1+1)(w_4-w_2)}; W\right] \\ &\quad \left. + 2w_3w_2(w_4-w_1) \Pi\left[\frac{w_4(w_1-w_2)}{w_1(w_4-w_2)}; W\right] \right\}, \quad (\text{B4}) \end{aligned}$$

in which we used $E(\pi/2; q) = E(q)$, $F(\pi/2; q) = K(q)$ and $\Pi(p; \pi/2; q) = \Pi(p, q)$ [20].

APPENDIX C: CUBIC INTERPOLATION

In Section III, we use the analytic approximation for $\sigma(x)$ in Eq. (24) which involves the cubic interpolation

$$\sigma = C_0 + C_1 x + C_2 x^2 + C_3 x^3, \quad (\text{C1})$$

$$C_0 = \kappa_1 x_1 \frac{(2\sqrt{D}-1) \kappa_2^2 x_2^2 (\kappa_2 x_2 - \kappa_1 x_1) - 2\sqrt{D} \ln(2\sqrt{A}) \kappa_1 x_1 (3\kappa_2 x_2 - \kappa_1 x_1)}{2\sqrt{D} (\kappa_2 x_2 - \kappa_1 x_1)^3} \quad (\text{C2a})$$

$$C_1 = \frac{(\kappa_2 x_2 - \kappa_1 x_1) [\kappa_2 x_2 (2\kappa_1 x_1 + \kappa_2 x_2) - 2\sqrt{D} \kappa_1 x_1 (4\kappa_2 x_2 - \kappa_1 x_1)] + 12\sqrt{D} \ln(2\sqrt{A}) \kappa_1 \kappa_2 x_1 x_2}{2\sqrt{D} (\kappa_2 x_2 - \kappa_1 x_1)^3} \quad (\text{C2b})$$

$$C_2 = \frac{6\sqrt{D} \ln(2\sqrt{A}) (\kappa_1 x_1 + \kappa_2 x_2) + (2\sqrt{D}-1) (\kappa_1^2 x_1^2 + \kappa_1 \kappa_2 x_1 x_2 - 2\kappa_2^2 x_2^2)}{2\sqrt{D} (\kappa_1 x_1 - \kappa_2 x_2)^3} \quad (\text{C2c})$$

$$C_3 = \frac{4\sqrt{D} \ln(2\sqrt{A}) - (2\sqrt{D}-1) (\kappa_2 x_2 - \kappa_1 x_1)}{2\sqrt{D} (\kappa_2 x_2 - \kappa_1 x_1)^3}. \quad (\text{C2d})$$

Finally, one can express everything in terms of the original parameters $\tilde{\omega}$ and ℓ by making use of Eqs. (20a)-(20c).

for $\kappa_1 x_1 < x < \kappa_2 x_2$. The above coefficients C_i , with $i = 0, \dots, 3$, can be easily expressed in terms of the parameters A , B and D for the Morse potential (18) as

-
- [1] S. Chandrasekhar, *The mathematical theory of black holes*, Oxford University Press, Oxford (1992).
- [2] N.D. Birrell and P.C.W. Davies, *Quantum fields in curved space*, Cambridge University Press, Cambridge (1982).
- [3] S.W. Hawking, *Nature* **248**, 30 (1974); *Comm. Math. Phys.* **43**, 199 (1975).
- [4] H.P. Nollert, *Class. Quantum Grav.* **16**, R159 (1999).
- [5] S.A. Teukolsky, *Astrophys. J.* **185**, 635 (1973).
- [6] H.A. Kramers, *Z. Phys.* **39** 836 (1926); L.A. Young and G.E. Uhlenbeck, *Phys. Rev.* **36** 1158 (1930).
- [7] R.E. Langer, *Phys. Rev.* **51**, 669 (1937).
- [8] S. Iyer and C.M. Will, *Phys. Rev. D* **35**, 3621 (1987).
- [9] J. Grain and A. Barrau, *Nucl. Phys. B* **742**, 253 (2006)
- [10] R. Casadio, F. Finelli, M. Luzzi and G. Venturi, *Phys. Rev. D* **71**, 043517 (2005)
- [11] R.B. Dingle, *Appl. Sci. Res. B* **5**, 345 (1956).
- [12] S.C. Miller and R. H. Good, *Phys. Rev.* **91**, 174 (1953).
- [13] M.V. Berry and K.E. Mount, *Rep. Prog. Phys.* **35**, 315 (1972).
- [14] R. Casadio, F. Finelli, A. Kamenshchik, M. Luzzi and G. Venturi, *JCAP* **0604**, 011 (2006).
- [15] A. Kamenshchik, M. Luzzi and G. Venturi, *Remarks on the method of comparison equations (generalized WKB method) and the generalized Ermakov-Pinney equation*, math-ph/0506017.
- [16] C.E. Hecht and J.E. Mayer, *Phys. Rev.* **106**, 1156 (1957).
- [17] H. Moriguchi, *J. Phys. Soc. Japan* **14**, 1771 (1959).
- [18] P. Pechukas, *J. Chem. Phys.* **54**, 3864 (1971).
- [19] G. Rawitscher, C. Merow, M. Nguyen and I. Simbotin, *Am. J. Phys.* **70**, 935 (2002)
- [20] M. Abramowitz and I. Stegun, *Handbook of mathematical functions with formulas, graphs, and mathematical table*, Dover Publishing, Dover (1965).
- [21] P. Kanti and J. March-Russell, *Phys. Rev. D* **66**, 024023 (2002).
- [22] P.C. Argyres, S. Dimopoulos and J. March-Russell, *Phys. Lett. B* **441**, 96 (1998); R. Casadio, A. Fabbri and L. Mazzacurati, *Phys. Rev. D* **65**, 084040 (2002); R. Casadio and L. Mazzacurati, *Mod. Phys. Lett. A* **18**, 651 (2003).
- [23] S. Dimopoulos and G. Landsberg, *Phys. Rev. Lett.* **87**, 161602 (2001); R. Casadio and B. Harms, *Int. J. Mod. Phys. A* **17**, 4635 (2002); G. L. Alberghi, R. Casadio, D. Galli, D. Gregori, A. Tronconi and V. Vagnoni, "Probing quantum gravity effects in black holes at LHC," hep-ph/0601243.
- [24] A similar coordinate was already used in Ref. [21].
- [25] Of course, if we are interested in setting the initial conditions at $x_0 \gg x_2$ the expressions must be adjusted correspondingly.